

A study on loops and eddies identified from the trajectories of drifters in the North Indian Ocean

Shrikant Dora ^{a,b}, S. G. Aparna ^{a,b,*}

^aCSIR-National Institute of Oceanography, Dona Paula, Goa-403004, India

^bAcademy of Scientific and Innovative Research (AcSIR), Ghaziabad-201002, India

*Corresponding author: Dr. S. G. Aparna, Email: aparna@nio.org

Abstract

We identify loops and eddies from the trajectories of the drifters in the North Indian Ocean (NIO) from October 1985 to March 2019. We use geometric identification method for loops and eddies and compare them with the loops identified from loopers provided by Lumpkin (2016). In NIO, the number of loops estimated from loopers is less than the number of loops and eddies identified by the geometric identification method. A total of 761 loops are identified, of which 346 are eddies, whereas the loops identified from loopers are only 149. Larger radii loops and eddies are observed in the western and central Bay of Bengal (BoB) and the southwestern part of the Arabian Sea (AS). Temporal variation of loops and eddies shows a peak during April-May in the AS and September-October in the BoB. In the BoB, the temporal variation of cyclonic eddies matches with the variation in chlorophyll.

Keywords: Drifters, Trajectories, Eddies, Arabian Sea, Bay of Bengal, North Indian Ocean

1.Introduction

North Indian Ocean (NIO), owing to the closed boundary in the north, possesses a unique circulation pattern. The seasonal reversal of winds and the associated changes in the seasonal circulation patterns in the NIO have become an interesting topic for many researchers. Most studies encompassing surface circulation in the NIO are either based on satellite data products (Peng et al., 2015; Raj, 2017) or the numerical models (Kantha et al., 2008; Sengupta et al., 2007; Vinayachandran and Kurian, 2008) or both (Shankar et al., 2002). Very few studies have incorporated drifters to study surface circulation in the NIO. Unlike model or satellite-based data products that are gridded and have continuous time-series, drifter data are patchy and lack continuity at a particular location as the location of the drifters change with time. Hence, there are fewer studies using drifters compared to other datasets. A few of the early studies using drifter's data were carried out by Molinari et al. (1990); Shenoi et al. (1999) to study the surface circulation in the tropical Indian Ocean. Beal et al. (2013) used both satellite and drifter's data to study the response of the Surface Circulation of the Arabian Sea (AS) to monsoonal forcing. Recently, Hormann et al. (2016) deployed an array of drifters to study the horizontal advection of freshwater at various spatio-temporal scales in the northern Bay of Bengal (BoB). Further, Hormann et al. (2019) used drifter and Argo float observations data to study freshwater export pathways from BoB into the Indian Ocean and the Arabian Sea. In another study using drifter's data, Dora et al. (2020) described the flow characteristics from the trajectories of three drifters deployed simultaneously at the same location in the northeastern AS.

The trajectories of the drifters have also been used in the study of oil spills (Liu et al., 2011; Price et al., 2006) and particle tracking techniques (Putman and He, 2013). Since the drifters follow the nature of ocean flow, their trajectories undergo loops and turns depending on the instantaneous magnitude and direction of the current. For example, when a drifter is trapped in an eddy, it makes either a cycloidal or a looping trajectory; these loops can be associated with eddies. The eddies smaller than 40 km are difficult to be identified from satellite-derived sea level fields. These sub-mesoscale eddies also play a key role in biogeochemical budgets through intense upwelling of nutrients, subduction of plankton, and horizontal stirring (Ledwell et al., 1993; Lévy and Klein, 2004; Zheng et al., 2015).

Various studies have used loops from trajectories of the drifters to study eddy characteristics. Loops are identified as the closed or near closed segments in the trajectories. One of the most common techniques to identify loops is the geometric identification method (Li et al., 2011; Zheng et al., 2015). In this method, the closed or near closed segments in the drifter trajectories are identified as loops. Not all loops are eddies, and a loop is considered to be an eddy only if two or more consecutive loops with the same polarity are observed along the same drifter's trajectory. Li et al. (2011) studied the eddies in

the South China Sea (SCS) and observed that around 70 % of the observed eddies are anticyclonic. They also identified that the temporal distribution of the number of eddies in the northern SCS has a close relationship with the Asian monsoon. Zheng et al. (2015) have statistically investigated the cyclonic and anticyclonic eddies from sub-mesoscale to mesoscale in the South Indian Ocean (SIO). They found that of the total eddies identified in the SIO, 60 % were anticyclonic and inferred that the mesoscale eddies showed significant seasonal variability.

Dong et al. (2011) have applied an additional criterion for a loop to be eddy. They rejected all the loops that have periodicities beyond 1-90 days. Based on this additional criterion, eddies are identified from the set of loops. Dong et al. (2011) in the Kuroshio extension region showed that 52 % of the total eddies identified are anticyclonic eddies. The spatial distribution of these eddies suggests that eddy abundance is highest along the Kuroshio path. Recently, Lumpkin (2016) has suggested that the methodology adopted by Dong et al. (2011) identifies any closed trajectory segments as loops, regardless of how irregular the trajectory is during that segment. Lumpkin (2016) identifies the loopers consisting of two or more loops using a methodology that would detect segments of drifter trajectories that exhibit sustained looping with a particular spin. He identified the loopers in the world basins and associated them with eddies identified by the satellite altimetry.

The method followed by Lumpkin (2016) is more stringent for the circular path to be identified as a looper and then as an eddy. In the Kuroshio extension region, Dong et al. (2011) identified 1808 eddies using drifter trajectories during 1979-2009, whereas 682 loops (drogued and undrogued) were identified from loopers provided by Lumpkin (2016) for a much longer period 1979–2019.

Do such differences in statistics between the two methods are confined only to a particular region? Do these two methods show different statistics of eddies in the NIO also? Are these loops and eddies uniformly distributed over the entire basin? Does the number of loops and eddies have a seasonal variation? The number of eddies in the NIO is reported to vary in space and time. The spatio-temporal variability of eddies in the NIO is studied by various authors. For example, Trott et al. (2018) showed that the number of cyclonic and anticyclonic eddies peak during pre-monsoon in the western AS. During the winter monsoon, weaker eddy activity is observed. Cheng et al. (2013) identified eddies using the satellite sea-level data and detected two distinct bands of high eddy activity region in western and central BoB. Another study by Mukherjee et al. (2019) in the BoB showed that during spring, the eddy activity is weaker in the BoB compared to summer and winter. However, all the above studies on spatio-temporal variability are either based on satellite altimetry and/or model studies. Do the loops and eddies identified using the drifters' trajectories also show a similar trend?

To answer the above questions, in the present study, we identify loops from the drifter trajectories in the NIO, following the method of Dong et al. (2011), and compare them with the loops estimated from loopers identified by Lumpkin (2016) in the NIO. Furthermore, we compare the statistics and the characteristics of these loops with that of eddies in the NIO. We also describe the spatio-temporal characteristics of the loops and eddies identified from both the methods and compare them with the earlier studies, which were based on the satellite data and model outputs.

2. Data and methods

We used satellite-tracked drifter data in the NIO for the period October 1985 to March 2019. The total number of observations is shown in Figure 1. Quality controlled 6-hourly interpolated positions (Hansen and Poulain, 1996; Lumpkin and Centurioni, 2019) of drogued drifters are downloaded from <https://www.aoml.noaa.gov/phod/gdp/interpolated/data/subset.php>. The data availability during 1985-2019 in the grid size of $0.25^\circ \times 0.25^\circ$ is shown in Figure 1. Rossby radius of deformation values were taken as per Chelton et al. (1998) and downloaded from http://www-po.coas.oregonstate.edu/research/po/research/rossby_radius/. In the present study, the drifters west of 78°E are considered to be in the AS, and the drifters east of 78°E are considered to be in the BoB.

2.1. Identification of Loops (L1)

We followed Dong et al. (2011) in identifying a loop segment from a drifter trajectory. A schematic representation of this method to estimate a loop from the trajectory is shown in Figure 2a. Consider a point A in the trajectory at time t_0 , and let Q be the location of the drifter after some cut-off time step, say t_1 . The distance between point A and all other points on the trajectory from Q is calculated. If the trajectory forms a loop, then at a particular time, say t_n on n^{th} day, the drifter location (at point B) would be close to the point A . Consider a series of points in the drifter trajectory $S(i)$, where $i=1, 2, 3, \dots, M$; M is the total number of points in the drifter trajectory. At any given point $S(i)$, say point A along the drifter trajectory, the identification of the loop segment starts with estimating the distance $D(i, k)$ between point $S(i)$ and the successive points $S(k)$. If the trajectory contains a loop, then at a particular time, $D(i, k)$ will be less than the threshold distance D_0 . For example, when iteration starts at point A , the distance is calculated from point A to all succeeding points after point Q in the trajectory. Say at point B , the distance is less than the threshold, then all the points from point A to B is considered to be in a loop. The threshold distance is to mark the distance when the drifter is returning to its former location.

Apart from the distance, we put a condition on the minimum and maximum time period during the trajectory that should have made a loop. The searching range is $[i + \tau, \min(i + N, M)]$, where τ is the

cut-off time step, and N is the maximum time limit to search a loop. Thus, for the first part of loop identification, the following conditions should satisfy:

$$D(i, k) \leq D_0$$

$$i + \tau < k < \min(i + N, M)$$

If these two conditions are not satisfied at point $S(i)$, then the iteration moves to the next step $S(i+1)$, and the search goes on. And if a loop segment is identified, the next iteration starts from the point succeeding the last point of the loop segment. In this study, for identifying loops, we have chosen the cut-off period (τ) of 6 days for initiation of search and the maximum search time of 90 days. The lower cut-off of 6 days is chosen to filter out the inertial oscillations. The inertial time period, T is given by $2\pi/f$, where the local inertial frequency $f = 2\Omega \sin(A)$, A is the latitude, and Ω is the earth rotating frequency. For latitudes 5°N to 25°N , T varies from ~ 5.7 days to ~ 1.2 days. Hence the lower cut-off is chosen as 6 days. The higher cut-off for the search is chosen as 90 days following Dong et al. (2011), a longer search time might result in a trajectory segment of a flow gyre that is taken as an eddy; a shorter search time might exclude some eddies that have a long rotating period. These cut-offs will exclude loops with periods shorter than that of the local inertial periods and longer than intra-seasonal periods.

The threshold distance (D_0) is taken as 5 km; reducing the threshold distance reduces the number of loops. A threshold distance of 10 km, 5 km, and 3 km gave 876, 761, and 608 loops respectively in the NIO.

The next step is the determination of the rotating angle θ , and the polarity of the loop segment. The polarity of the loops is used to identify cyclonic and anticyclonic loops. Both rotating angle and polarity are determined using the loop center. Once the loop is identified, the loop center is estimated by averaging all the points consisting of latitudes and longitudes in the drifter loop trajectory. Angle is then calculated between the adjacent points from the loop center to determine the rotating angle, θ (Figure 2a). Ideally, the total rotating angle θ should be close to 360° . The looping segment can finally be considered to be a loop when θ is greater than θ_0 ($\sim 300^\circ$). Polarity is determined by the sign of the angle. For the northern hemisphere, a cyclonic loop traverses anticlockwise (positive), and an anticyclonic loop follows the clockwise direction (negative). So, the segment that satisfies the three criteria i.e., the minimum threshold distance, searching time period, and rotating angle, can be considered as a loop. The loop radius is given as the mean distance between all the loop points from the loop center. Mean tangential velocity for the loop was determined by averaging current along all the points in the loop. For our study, we have taken the region north of the equator as the area of

interest. So, the loops with center points that are above the equator are taken into account. We shall be using the term "L1" for all the loops identified (Figure 3a).

2.2. Identification of Eddies (E1)

Not all the L1 loops are associated with eddy flow. So, two or more loops are deemed eddy only if they are within advection distance and have the same polarity (Dong et al., 2011). The distance between the loop centers of the two loops $D_{loopcenter}$, should always be less than the net advection distance D_{adv} , which is estimated using the average current along two loops and time interval between two loops.

$$D_{loopcenter} < D_{adv}$$

For example, in Figure 2b, only a single loop is observed in the trajectory of the drifter with DAC No. 27051 and WMO Id. 2300507 (DAC Nos. and WMO Ids. are identification numbers assigned to each drifter at Atlantic Oceanographic and Meteorological Laboratory (AOML), under the guidance of the World Meteorological Organization (WMO)). Hence, by definition, this loop shown in Figure 2b is not considered as an eddy. Figure 2c shows that the trajectory of the drifter (DAC No. 2134711 and WMO Id. 2300643) traces three loops. The centers of the three loops are within the limit of the advection distance. Hence it is considered as an eddy by definition. Since all the three loops are within the advection distance, statistically, these are considered as three eddies. We name these loops as "E1".

2.3. Loopers (L2)

Loopers i.e., looping segments in the drifter trajectory, are identified by Automatic Looper Detection. This method would detect trajectories of drifters which exhibited sustained looping with a particular spin. For more details see Lumpkin (2016). Loopers are looping segments that have completed two or more orbits in the drifter trajectory. Loopers data is downloaded from <https://www.aoml.noaa.gov/phod/loopers/>. We identified loops from these looper trajectories using the geometric identification method and termed it as "L2". Since loopers exhibit coherent vortices, any loop identified in the looping trajectory is considered as an eddy. The trajectory shown in Figure 2c satisfies the criteria for all the cases; it is a loop (L1), an eddy (E1), and also a loop from looper (L2).

2.4. Comparison of the methods

The loopers have stringent identification condition and hence are very less in number compared to loops and eddies identified by the geometric identification method. Since the direction of the spin does not change in the trajectory, loopers are smoother in shape compared to the loops and eddies. For example, the trajectory of the drifter (DAC No. 15710, WMO Id. 2300593) shown in Figure 4 is

identified as a loop L1 and also as an eddy E1, but not as L2. The drifter was deployed on 28 September 2002, and during the period of around 9 months, it traced two different eddies, as shown in the sea-level field. At the location 16°N and 89°E (given by an arrow), the direction of the rotation in the trajectory changes, which could be the possible reason for not being detected as a loop. However, even though it is identified as a loop and an eddy, the actual trajectory is because of the two circulation features as shown by the sea level and not a single eddy. In such cases, all the three methods have a drawback, that the first two methods identified a single loop and an eddy in the trajectory, though they are two different loops. It is not considered as a loop, as by definition, it requires at least two or more loops to be identified as a loop. The trajectory shown in Figure 2b is a loop but not an eddy, as it is not associated with a second loop within the advection distance. The sea-level field also shows a single circulating feature in this trajectory (Figure not shown). The loops, eddies, and the loopers identified from the trajectories correlate with the sea-level field, suggesting the robustness of these methods. The major advantage of these methods is the eddies with smaller radii or size that could not be identified in the sea-level field can be identified in the trajectories.

3. Results

Loops (L1), eddies (E1) are identified from the drifter trajectory for the period 1985–2019 following Dong et al. (2011). Loops (L2) are identified from looper trajectories downloaded from <https://www.aoml.noaa.gov/phod/loopers/>. In this section, we describe the statistics of L1, E1, and L2 in the NIO.

3.1. Statistics of loops

A total of 761 loops (L1) are identified from drifter trajectories in the NIO, with loop centers above the equator. Of the 761 L1 loops, 322 loops are in the BoB and 439 loops in the AS (Figure 3a). The loops (L1) are clustered around the western BoB and southwestern AS. The eastern AS (along the west coast of India) is nearly devoid of loops. The cyclonic and anticyclonic loops (L1) appear to be distributed equally in space, but the number of anticyclonic loops is slightly higher than that of cyclonic loops. Out of 761 loops (L1) in the NIO, 404 are anticyclonic, and 357 are cyclonic. In the AS, anticyclonic and cyclonic loops (L1) are 240 (55 %) and 199 (45 %), respectively. The numbers are not very different for the BoB, with 164 (51 %) anticyclonic and 158 (49 %) cyclonic loops.

The eddies (E1) are consecutive loops from the same drifter trajectory that satisfied two additional conditions (i) same polarity and (ii) advection distance between the two loop centers is less than the average distance covered by the loops and are shown in Figure 3b. The number of eddies reduced nearly to half of the L1 loops. There are 346 eddies (E1) in the NIO, of which 191 are anticyclonic and

155 are cyclonic respectively. There are 222 eddies in the AS with 130 (59 %) anticyclonic and 92 (41 %) cyclonic eddies. For the BoB, the number of eddies is 124, with 61 (49 %) anticyclonic and 63 (51 %) cyclonic eddies.

The L2 loops estimated from loopers identified by Lumpkin (2016) are very less in number compared to L1 loops and E2 eddies (Figure 3c). In total, 170 loopers were identified in the NIO, of which only 102 loopers were drogued. 149 loops were identified from drogued loopers using same condition as L1. Since each looper contains two or more loops, the total number of loops (L2) in the NIO is more than the number of loopers. Out of these 149 loops (L2), 100 (67.1 %) were cyclonic and 49 (32.9 %) were anticyclonic loops.

3.2. Size of the loops

The histogram of the loop radii for the NIO, AS, and the BoB is shown in Figure 5. It can be observed that drifters have the ability to characterize the sub-mesoscale eddies and loops that are unresolved by satellite altimeter data. The loops (L1) with radii less than 20 km are much higher in number than the loops with larger radii (Figures 5a, b, c). The mean radii of the anticyclonic loops (L1) for the NIO, AS, and the BoB are 61 km, 60.1 km, and 62.4 km respectively. The mean radii of the cyclonic loops (L1) for the NIO, AS and the BoB are 56.4 km, 54.9 km, and 58.3 km, respectively, and are shown in Table 1. The L1 loops in the AS have lower mean radii compared to the BoB.

The mean radii of the eddies (E1) also show similar trends; the eddies (E1) with smaller radii are higher in number (Figures 5d, e, f). The mean radii of the eddies for the NIO, AS and the BoB are 56 km, 55.5 km, and 56.7 km respectively. The mean radii of the cyclonic eddies (E1) for the NIO, AS and the BoB are 51.8 km, 50.6 km, and 53.6 km respectively. The mean radii of the anticyclonic eddies (E1) for the NIO, AS and the BoB are 59.4 km, 59.1 km, and 59.9 km respectively, and are shown in Table 1. The radius of the loop gives an indication of the size of the loop or an eddy. The eddy sizes are underestimated as drifter may be trapped in a part of an eddy. As discussed in Chaigneau and Pizarro (2005); Li et al. (2011), if drifters are statistically evenly distributed over an eddy of radius R , the probability density $p(r, \theta)$ of finding the drifter at a radius r and direction θ relative to the eddy center is constant. So,

$$p(r, \theta) = \frac{1}{\int_0^R \int_0^{2\pi} r dr d\theta} = \frac{1}{\pi R^2}$$

The mean distance $\overline{R_1}$, or the expectation

$$E(r) = \int_0^R \int_0^{2\pi} r^2 p(r, \theta) dr d\theta$$

of the drifter from the eddy center is given by $\overline{R_1} = 2R/3$. The mean radius $\overline{R_1}$ for all E1 eddies in the NIO, AS, and the BoB is 56 km, 55.5 km, and 56.7 respectively. So, on an average, an eddy of 56 km radius identified from the drifter loop is associated with an eddy radius of 84 km. The average radii of eddies in the BoB is reported to be around 90 km (Cui et al., 2016). It is slightly larger than the mean radii estimated from the drifter trajectories. This average by Cui et al. (2016) is based on the satellite-derived data that can detect the eddies that are greater than 30-40 km radii. Similarly, Chen et al. (2012) observed that the radii of the eddies identified using the satellite data is larger than the Rossby radius of deformation. This is well expected as the radius of the eddies identified using drifter is smaller compared to the eddies identified by the satellite data. Li et al. (2011) have observed that in the South China Sea (SCS), the eddy radius (estimated using drifter data) is an order of magnitude lower than the Rossby radius of deformation. We also observe the eddy radius south of 14°N is lower than the Rossby radius of deformation, as the Rossby radius of deformation increases rapidly towards the equator (Figure 6). At latitude 16°N (21-24°N), the eddy radius is slightly larger than the Rossby radius in the BoB (NIO and AS). The Rossby radius of deformation is often associated with the eddy size to understand the eddy dynamics (Chelton et al., 2007; Chen et al., 2012).

The L2 loops are very less in number. The loops (L2) with radii less than 20 km are much higher in number compared to the loops with larger radii (Figures 5g, h, i). The mean radii of the anticyclonic L2 loops for the NIO, AS, and the BoB are 41.46 km, 41.1 km, and 41.6 km respectively. The mean radii of the cyclonic L2 loops for the NIO, AS, and the BoB are 22.8 km, 20.4 km, and 25.1 km respectively, with mean radii of the cyclonic L2 loops for NIO, AS, and BoB being 41.4 km, 41.1 km, and 41.6 km and are shown in Table 1.

3.3. Spatio-temporal variability of loops and eddies

Figure 7 shows the spatial distribution of cyclonic and anticyclonic L1 loops and E1 eddies in the NIO. The loops and eddies are shown in circles corresponding to their radii. Thus, different sizes of circles show variable radii, with larger loops/eddies corresponding to larger radii and vice-versa. The density of the larger radii loops (L1) and eddies (E1) is higher in the western and central BoB. In the AS, most of the larger radii loops are seen in the southwestern part of the AS. The number of eddies is higher along the western and northern BoB compared to southern BoB.

There are no eddies observed in the eastern BoB (Figure 8). The eastern AS as well is nearly devoid of eddies. In both regions, the number of anticyclonic eddies is more than the cyclonic eddies. Not only the spatial variability but the number of the loops also vary with seasons and respond to the seasonal changes that occur in the NIO. To understand the seasonal changes in loops and eddies, we

analyzed our results for two seasons Summer Monsoon (June–September) and Winter Monsoon (November–February). There is a striking difference in the variation of loops and eddies in the northern and southern BoB; hence we looked into seasonal variation in the northern and southern bay. The region north of 16°N in the BoB is considered as northern BoB (NBoB) and the region south of 16°N is considered as southern BoB (SBoB). Figure 9 shows the histogram of the number of the loops and eddies during Summer Monsoon (SM) and Winter Monsoon (WM). During SM, anticyclonic eddies are higher compared to WM in the AS, BoB, and the SBoB. In the NBoB, the anticyclonic loops and eddies are high during WM. The number of anticyclonic loops and eddies is higher than the cyclonic loops and eddies during SM in the AS. A similar trend is observed for the SBoB, however in the NBoB; the cyclonic are higher than the anticyclonic eddies during SM.

The cyclonic loops and eddies are known to be highly productive and are likely to be generated by positive wind stress curl. Hence, we look into the variability of loops and eddies in association with variation in chlorophyll and wind stress curl. The number of cyclonic loops is high in the northwestern and central BoB (Figure 10a, b), both during SM and WM. The positive wind stress curl (favorable for cyclonic eddies) is observed along the northwest BoB during SM (Figure 10g). The chlorophyll in these regions is also high compared to the central BoB during SM (Figure 10e). The Gulf of Aden in the western AS is dominant with cyclonic loops during SM, where high chlorophyll and positive wind stress curl is observed. Southern (Northern) AS has more cyclonic loops during summer (winter) monsoons. The number of eddies is less compared to the number of loops in both the AS and the BoB. However, this decrease in the number is more prominent in the AS. During WM, the wind stress curl is negative (not favorable for cyclonic eddies) though a high number of cyclonic loops and eddies are observed along the northwestern BoB (Figure 10b, h), and also high chlorophyll is observed along the northwestern BoB (Figure 10h).

3.3.1 Temporal variability

A seasonal cycle is observed in the number of loops and eddies in the NIO. During April-May, the loops (L1) and eddies (E1) show a peak in the NIO (Figure 11a, f) and AS (Figure 11b, g). A minor peak is observed during September. In the AS, a third peak is observed during November–December (Figure 11g). The anticyclonic loops show a pattern similar to the total number of loops; however, the cyclonic loops and eddies remain nearly invariant in the NIO and the AS. BoB has a slightly different pattern from the NIO and the AS; the major peak is observed during September-October in both loops and eddies (Figure 11c, h), and the minor peak is observed during December-January in eddies (Figure 11h). But the number of L1 loops and E1 eddies show a dip during February in the NIO, AS, and the BoB. The seasonal variation in L1 and E1 is nearly the same, except that the number of eddies is less

than the number of loops. However, the loops (L2) differ in seasonal variation. They show a peak during December–January in all the regions NIO, AS, and the BoB (Figure 11k, l, m). The number of loops (L2) during June–September almost remains invariant. In the SBoB, the major peak in loops and eddies is observed during August–September, and the minor peak is observed during December–January (Figure 11e, j). In the NBoB, a sharp peak is observed during September (Figure 11d, i). Since cyclonic eddies are known to enhance chlorophyll, thereby production in the BoB (Prasanna et al., 2004), we look for the seasonal cycle of the number of cyclonic eddies and chlorophyll.

The temporal variation of the number of cyclonic eddies in the BoB matches the temporal variation of chlorophyll (Figure 12). The number of eddies and the chlorophyll have lower values during February–May compared to June–September. The number of eddies and the chlorophyll values show an increasing trend from June. A dip is observed in both chlorophyll and the number of eddies during October–November. The correlation coefficient is 0.52 and is significant at a 90 % confidence level. In the AS, such a match between the number of eddies and the chlorophyll is not observed. The possible reason could be that the chlorophyll in the AS is majorly determined by the upwelling phenomenon (Hood et al., 2017), whereas the BoB is an eddy dominant region; hence the chlorophyll in the the BoB is better correlated (Singh et al., 2015).

4. Discussion and Summary

Trajectories of drifters are in general associated with the instantaneous flow characteristics i.e., they are dependent on the instantaneous current at a particular location and time, and hence their trajectories possess an irregular shape. However, when analyzed over a larger period of time, the trajectories of some of the drifters follow a particular pattern; for example, when they are trapped in cyclonic or anticyclonic circulation features, they form a loop. Hence the trajectories of these drifters are used to study the loops and eddies in the oceans.

In the present study, we identify loops (L1) following Dong et al. (2011). Some of these loops satisfy the criteria suggested by Dong et al. (2011) to be eddies (E1). These criteria are listed in Table 1. Using a different method, Lumpkin (2016) identified loopers trajectories in which more than one loop are present. We extracted the loops L2 from these loopers using the geometric identification method.

More importantly, the statistics shown in Figure 5 shows that the smaller sized loops and eddies are much more in number compared to the larger radii loops and eddies. Though the drifters are not uniformly distributed in time and space, their data are available for more than 4 decades, which enables us to study such small size eddies/loops, which otherwise cannot be identified using satellite-based data products.

Our study shows that the loops and eddies show a strong seasonal cycle; they peak during the pre-monsoon season in the AS, a similar result was observed by Trott et al. (2018). They attributed this peak in the number of eddies to the wind-driven instability. The wind-stress curl during this season is negative in most of the AS basin. During SM, cyclonic loops in the northwestern part of the AS is associated with positive wind stress curl and high chlorophyll. This positive wind stress curl observed during SM is associated with the Findlater jet (Beal et al., 2013). Eddies with larger sizes tend to feature in the regions with large eddy kinetic energy (EKE) (Zheng et al., 2015). Our study shows that the Somalia region has larger radii eddies, which implies that the Somalia region should have high EKE. Sharma et al. (1999) has shown that the Somalia region has high EKE compared to the other regions in the AS.

In the BoB, the western bay is dominated by more eddies and larger radii. Cheng et al. (2013) highlighted two distinct bands of high eddy activity region in the western and central BoB. A similar result was earlier reported by Kurien et al. (2010). They attributed a high number of eddies to the baroclinic instability in the western BoB. Mukherjee et al. (2019) observed that region lying between 85-90°E and 18-21°N (defined as the NWBoB) has more eddies compared to the region 80-85°E and 10-13°N (defined as the SWBoB). Our study also shows that the NWBoB has more eddies than the SBoB. They observed that the number of cyclonic eddies is more compared to the anticyclonic eddies, but Dandapat and Chakraborty (2016); Roman-Stork et al. (2019) observed that in the BoB, anticyclonic eddies are more than cyclonic eddies. Though all the three studies are based on satellite data, they have used different methods of eddy identification and during different time periods. Our study shows that in the NIO, AS, and the BoB, anticyclonic eddies are more than cyclonic eddies. During SM, positive wind-stress curl is observed in the northwestern part of BoB, and so also the cyclonic eddies/loops associated with high chlorophyll. A similar result was observed by Dandapat and Chakraborty (2016). However, during certain times, though negative wind stress curl was observed, the cyclonic eddies were present. For example, in Figure 10, during WM, though negative wind stress curl is seen, along the western BoB, the cyclonic eddies are also present. This is because the wind stress curl is not the only reason for eddy generation. Roman-Stork et al. (2019) observed that high eddy generation in the eastern BoB is associated with instability induced by coastal Kelvin waves and the westward propagating Rossby waves.

In summary, we identify the loops and eddies from the trajectories of the drifters in the NIO using two different methods. Depending on the method used, there were slight changes observed in the statistics of the loops and eddies. The statistics and spatio-temporal variability of loops and eddies identified in this study match well with earlier reported studies, suggesting that these methods are reliable and can

be used for characterizing the eddies in the region. The comparison with the satellite-based studies is important for this study, as the drifter's data is not evenly distributed in space and time. In spite of being non-uniform distribution, the drifter data has a unique advantage over the satellite-based studies is that the loops and eddies of smaller sizes (< 40 km) can also be identified along with the larger radii. Spatio-temporal variability studies of the loops/eddies of such smaller sizes were not done earlier in the NIO for such a long time period. However, the unequal distribution would remain as a lacuna for any studies using the drifter data. It would always remain as a drawback for such studies and would pose a challenge working with these data sets.

Acknowledgements

Shrikant Dora acknowledges the Academy of Scientific and Innovative Research (AcSIR) and the financial support from Council of Scientific and Industrial Research (CSIR), India and ESSO-Indian National Centre for Ocean Information Services (INCOIS), Hyderabad, India. The Drifter project has been supported by grants from the Ministry of Earth Sciences (MoES, via INCOIS) through its programme on Ocean Observing Networks. We also acknowledge the ship time provided by CSIR–NIO for drifter deployment. We also thank Rahul Khedekar and Dr. Vineet Jain for their inputs during discussions. The figures have been plotted using Ferret and Python. This is CSIR-NIO contribution
xxxx.

References

- Beal, L. M., Hormann, V., Lumpkin, R., Foltz, G. R., 2013. The response of the surface circulation of the Arabian Sea to monsoonal forcing. *J. Phys. Oceanogr.* 43 (9), 2008–2022. <http://dx.doi.org/10.1175/JPO-D-13-033.1>
- Chaigneau, A., Pizarro, O., 2005. Eddy characteristics in the eastern South Pacific. *J. Geophys. Res.-Oceans* 110 (C6). <http://dx.doi.org/10.1029/2004JC002815>
- Chelton, D., Schlax, M. G., Samelson, R. M., DeSzoeki, R. A., 2007. Global observations of large oceanic eddies. *Geophys. Res. Lett.* 34(15). <http://dx.doi.org/10.1029/2007GL030812>
- Chelton, D. B., DeSzoeki, R. A., Schlax, M. G., Naggar, K. E., Siwertz, N., 1998. Geographical variability of the first baroclinic rossby radius of deformation. *J. Phys. Oceanogr.* 28 (3), 433–460. [http://dx.doi.org/10.1175/1520-0485\(1998\)028%3C0433:GVOTFB%3E2.0.CO;2](http://dx.doi.org/10.1175/1520-0485(1998)028%3C0433:GVOTFB%3E2.0.CO;2)
- Chen, G., Wang, D., Hou, Y., 2012. The features and interannual variability mechanism of mesoscale eddies in the Bay of Bengal. *Cont. Shelf Res.* 47, 178–185. <http://dx.doi.org/10.1016/j.csr.2012.07.011>
- Cheng, X., Xie, S., McCreary, J. P., Qi, Y., Du, Y., 2013. Intraseasonal variability of sea surface height in the Bay of Bengal. *J. Geophys. Res.-Oceans* 118 (2), 816–830. <http://dx.doi.org/10.1002/jgrc.20075>
- Cui, W., Yang, J., Ma, Y., 2016. A statistical analysis of mesoscale eddies in the Bay of Bengal from 22-year altimetry data. *Acta Oceanol. Sin.* 35 (11), 16–27. <http://dx.doi.org/10.1007/s13131-016-0945-3>
- Dandapat, S., Chakraborty, A., 2016. Mesoscale eddies in the Western Bay of Bengal as observed from satellite altimetry in 1993–2014: statistical characteristics, variability and three-dimensional properties. *IEEE J. Sel. Top. Appl.* 9 (11), 5044–5054. <http://dx.doi.org/10.1109/JSTARS.2016.2585179>
- Dong, C., Liu, Y., Lumpkin, R., Lankhorst, M., Chen, D., McWilliams, J. C., Guan, Y., 2011. A scheme to identify loops from trajectories of oceanic surface drifters: An application in the Kuroshio Extension region. *J. Atmos. Ocean. Tech.* 28 (9), 1167–1176. <http://dx.doi.org/10.1175/JTECH-D-10-05028.1>
- Dora, S., Khedekar, R., Aparna, S. G., 2020. Trajectories of three drifters deployed simultaneously in the northeastern Arabian Sea. *J. Earth Syst. Sci.* 129 (1), 1–8. <http://dx.doi.org/10.1007/s12040-019-1292-5>
- Hansen, D. V., Poulain, P.-M., 1996. Quality control and interpolations of WOCE-TOGA drifter data. *J. Atmos. Ocean. Tech.* 13 (4), 900–909. [http://dx.doi.org/10.1175/1520-0426\(1996\)013%3C0900:QCAIOW%3E2.0.CO;2](http://dx.doi.org/10.1175/1520-0426(1996)013%3C0900:QCAIOW%3E2.0.CO;2)
- Hood, R. R., Beckley, L. E., Wiggert, J. D., 2017. Biogeochemical and ecological impacts of boundary currents in the Indian ocean. *Prog. Oceanogr.* 156, 290–325. <http://dx.doi.org/10.1016/j.pocean.2017.04.011>
- Hormann, V., Centurioni, L. R., Gordon, A. L., 2019. Freshwater export pathways from the Bay of Bengal. *Deep-Sea Res. PT II* 168, 104645. <http://dx.doi.org/10.1016/j.dsr2.2019.104645>

- Hormann, V., Centurioni, L. R., Mahadevan, A., Essink, S., D'Asaro, E. A., Kumar, B. P., 2016. Variability of near-surface circulation and sea surface salinity observed from Lagrangian drifters in the northern Bay of Bengal during the waning 2015 southwest monsoon. *Oceanography* 29 (2), 124–133. <http://dx.doi.org/10.5670/oceanog.2016.45>
- Kantha, L., Rojsiraphisal, T., Lopez, J., 2008. The North Indian Ocean circulation and its variability as seen in a numerical hindcast of the years 1993–2004. *Prog. Oceanogr.* 76 (1), 111–147. <http://dx.doi.org/10.1016/j.pocean.2007.05.006>
- Kurien, P., Ikeda, M., Valsala, V. K., 2010. Mesoscale variability along the east coast of India in spring as revealed from satellite data and OGCM simulations. *J. Oceanogr.* 66 (2), 273–289. <http://dx.doi.org/10.1007/s10872-010-0024-x>
- Ledwell, J. R., Watson, A. J., Law, C. S., 1993. Evidence for slow mixing across the pycnocline from an open-ocean tracer-release experiment. *Nature* 364 (6439), 701–703. <http://dx.doi.org/10.1038/364701a0>
- Lévy, M., Klein, P., 2004. Does the low frequency variability of mesoscale dynamics explain a part of the phytoplankton and zooplankton spectral variability? *Philos. T. Roy. Soc. A* 460 (2046), 1673–1687. <https://doi.org/10.1098/rspa.2003.1219>
- Li, J., Zhang, R., Jin, B., 2011. Eddy characteristics in the northern South China Sea as inferred from Lagrangian drifter data. *Ocean Sci.* 7 (5), 661. <https://doi.org/10.5194/os-7-661-2011>
- Liu, Y., Weisberg, R. H., Hu, C., Kovach, C., Riethmüller, R., 2011. Evolution of the Loop Current system during the Deepwater Horizon oil spill event as observed with drifters and satellites. *Monitoring and Modeling the Deepwater Horizon Oil Spill: A Record-Breaking Enterprise*, *Geophys. Monogr. Ser* 195, 91–101. <https://doi.org/10.1029/2011GM001127>
- Lumpkin, R., 2016. Global characteristics of coherent vortices from surface drifter trajectories. *J. Geophys. Res.-Oceans* 121 (2), 1306–1321. <https://doi.org/10.1002/2015JC011435>
- Lumpkin, R., Centurioni, L., 2019. Global Drifter Program Quality-Controlled 6-hour Interpolated Data from Ocean Surface Drifting Buoys. NOAA National Centers for Environmental Information Dataset. <https://doi.org/10.25921/7ntx-z961>
- Molinari, R. L., Olson, D., Reverdin, G., 1990. Surface current distributions in the tropical Indian Ocean derived from compilations of surface buoy trajectories. *J. Geophys. Res.-Oceans* 95 (C5), 7217–7238. <https://doi.org/10.1029/JC095iC05p07217>
- Mukherjee, A., Chatterjee, A., Francis, P., 2019. Role of Andaman and Nicobar Islands in eddy formation along western boundary of the Bay of Bengal. *Sci. Rep.-UK* 9 (1), 1–10. <http://dx.doi.org/10.1038/s41598-019-46542-9>
- Peng, S., Qian, Y.-K., Lumpkin, R., Du, Y., Wang, D., Li, P., 2015. Characteristics of the near-surface currents in the Indian Ocean as deduced from satellite-tracked surface drifters. Part i: Pseudo-Eulerian statistics. *J. Phys. Oceanogr.* 45 (2), 441–458. <https://doi.org/10.1175/JPO-D-14-0050.1>
- PrasannaKumar, S., Nuncio, M., Narvekar, J., Kumar, A., Sardesai, S., deSouza, S. N., Gauns, M., Ramaiah, N., Madhupratap, M., 2004. Are eddies nature's trigger to enhance biological productivity in the Bay of Bengal? *Geophys. Res. Lett.* 31 (7). <https://doi.org/10.1029/2003GL019274>

- Price, J. M., Reed, M., Howard, M. K., Johnson, W. R., Ji, Z. G., Marshall, C. F., Jr., N. L. G., Rainey, G. B., 2006. Preliminary assessment of an oil-spill trajectory model using satellite-tracked, oil-spill-simulating drifters. *Environ. Modell. Softw.* 21 (2), 258–270. <https://doi.org/10.1016/j.envsoft.2004.04.025>
- Putman, N. F., He, R., 2013. Tracking the long-distance dispersal of marine organisms: sensitivity to ocean model resolution. *J. R. Soc. Interface* 10 (81), 20120979. <https://doi.org/10.1098/rsif.2012.0979>
- Raj, R. P., 2017. Surface velocity estimates of the north indian ocean from satellite gravity and altimeter missions. *Int. J. Remote Sens.* 38 (1), 296–313. <https://doi.org/10.1080/01431161.2016.1266106>
- Roman-Stork, H. L., Subrahmanyam, B., Trott, C. B., 2019. Mesoscale eddy variability and its linkage to deep convection over the Bay of Bengal using satellite altimetric observations. *Adv. Space Res.* <https://doi.org/10.1016/j.asr.2019.09.054>
- Sengupta, D., Senan, R., Goswami, B. N., Vialard, J., 2007. Intraseasonal variability of equatorial Indian Ocean zonal currents. *J. Climate* 20 (13), 3036–3055. <https://doi.org/10.1175/JCLI4166.1>
- Shankar, D., Vinayachandran, P., Unnikrishnan, A. S., 2002. The monsoon currents in the north Indian Ocean. *Prog. Oceanogr.* 52, 63–120.
- Sharma, R., Gopalan, A. K. S., Ali, M. M., 1999. Interannual variation of eddy kinetic energy from TOPEX altimeter observations. *Mar. Geod.* 22(4), 239–248. <https://doi.org/10.1080/014904199273371>
- Shenoi, S. S. C., Saji, P. K., Almeida, A. M., 1999. Near-surface circulation and kinetic energy in the tropical Indian Ocean derived from Lagrangian drifters. *J. Mar. Res.* 57 (6), 885–907. <https://doi.org/10.1357/002224099321514088>
- Singh, A., Gandhi, N., Ramesh, R., Prakash, S., 2015. Role of cyclonic eddy in enhancing primary and new production in the Bay of Bengal. *J. Sea Res.* 97, 5–13. <https://doi.org/10.1016/j.seares.2014.12.002>
- Trott, C. B., Subrahmanyam, B., Chaigneau, A., Delcroix, T., 2018. Eddy tracking in the northwestern Indian Ocean during southwest monsoon regimes. *Geophys. Res. Lett.* 45 (13), 6594–6603. <https://doi.org/10.1029/2018GL078381>
- Vinayachandran, P., Kurian, J., 2008. Modeling Indian ocean circulation: Bay of Bengal fresh plume and Arabian sea mini warm pool. In: *Proceedings of the 12th Asian Congress of Fluid Mechanics*. Citeseer, pp. 18–21.
- Zheng, S., Du, Y., Li, J., Cheng, X., 2015. Eddy characteristics in the South Indian Ocean as inferred from surface drifters. *Ocean Sci.* 11 (3), 361–371. <https://doi.org/10.5194/os-11-361-2015>

Table 1: Number and Radius of L1 and L2 loops, and E1 eddies. Total refers to total (combined cyclonic and anticyclonic) loops/eddies. Cyc and Anti refers to cyclonic and anticyclonic loops/eddies respectively.

	Conditions to be satisfied	Numbers									Radius (km)								
		NIO			AS			BoB			NIO			AS			BoB		
		Total	Anti	Cyc	Total	Anti	Cyc	Total	Anti	Cyc	Total	Anti	Cyc	Total	Anti	Cyc	Total	Anti	Cyc
L1	(i) Closed or near-closed loops (ii) Threshold distance < 5km (iii) Rotating angle (θ) > 300°	761	404	357	439	240	199	322	164	158	58.9	61	56.4	57.8	60.1	54.9	60.4	62.4	58.3
E1	(i) Two or more L1 loops (ii) Same polarity (iii) $D_{loopcenter} < D_{adv}$	346	191	155	222	130	92	124	61	63	56	59.4	51.8	55.5	59.1	50.6	56.7	59.9	53.6
L2	(i) Loops extracted from loopers	149	49	100	90	33	57	59	16	43	32.1	41.4	22.8	30.8	41.1	20.4	33.4	41.6	25.1

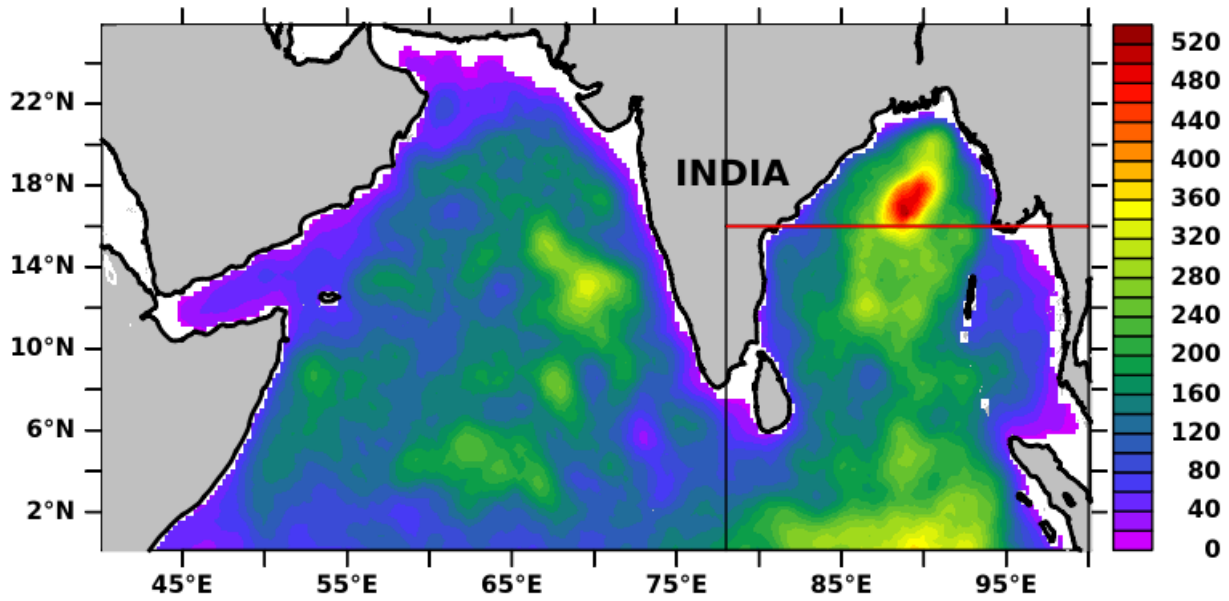


Figure 1. Number of 6-hourly observations of drifter locations during 1985–2019 in $0.25^\circ \times 0.25^\circ$ spatial grids. Region to the west of 78°E represents Arabian Sea (AS) and that to the right represents Bay of Bengal (BoB). The red line at 16°N divides the BoB into two regions (i) northern BoB (NBoB, north of 16°N) and (ii) southern BoB (SBoB, south of 16°N).

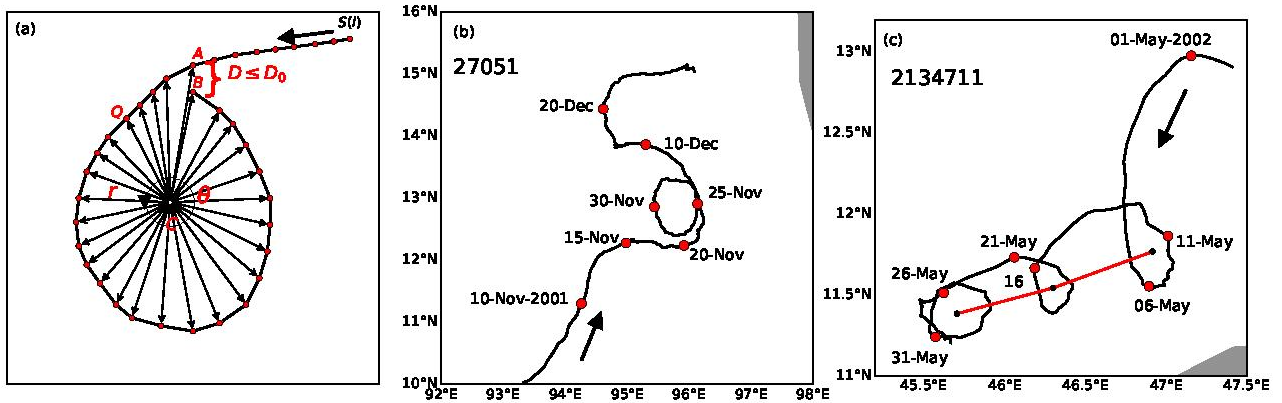


Figure 2. (a) A schematic representation for identifying a loop from the drifter trajectory, using the method of Dong et al. (2011). The point C is the loop center, r is the distance between center of loop to drifter positions, θ is rotating angle. A and B are starting and ending positions of the loop respectively and the distance between them is denoted by D . D_0 refers to threshold distance. Q is the position of the drifter after the cutoff period. (b) Trajectory of drifter (with DAC No. 27051 and WMO Id. 2300507) in which a L1 loop is identified. (c) Trajectory of drifter (with DAC No. 2134711 and WMO Id. 2300643) which shows L1, L2 loops and E1 eddies.

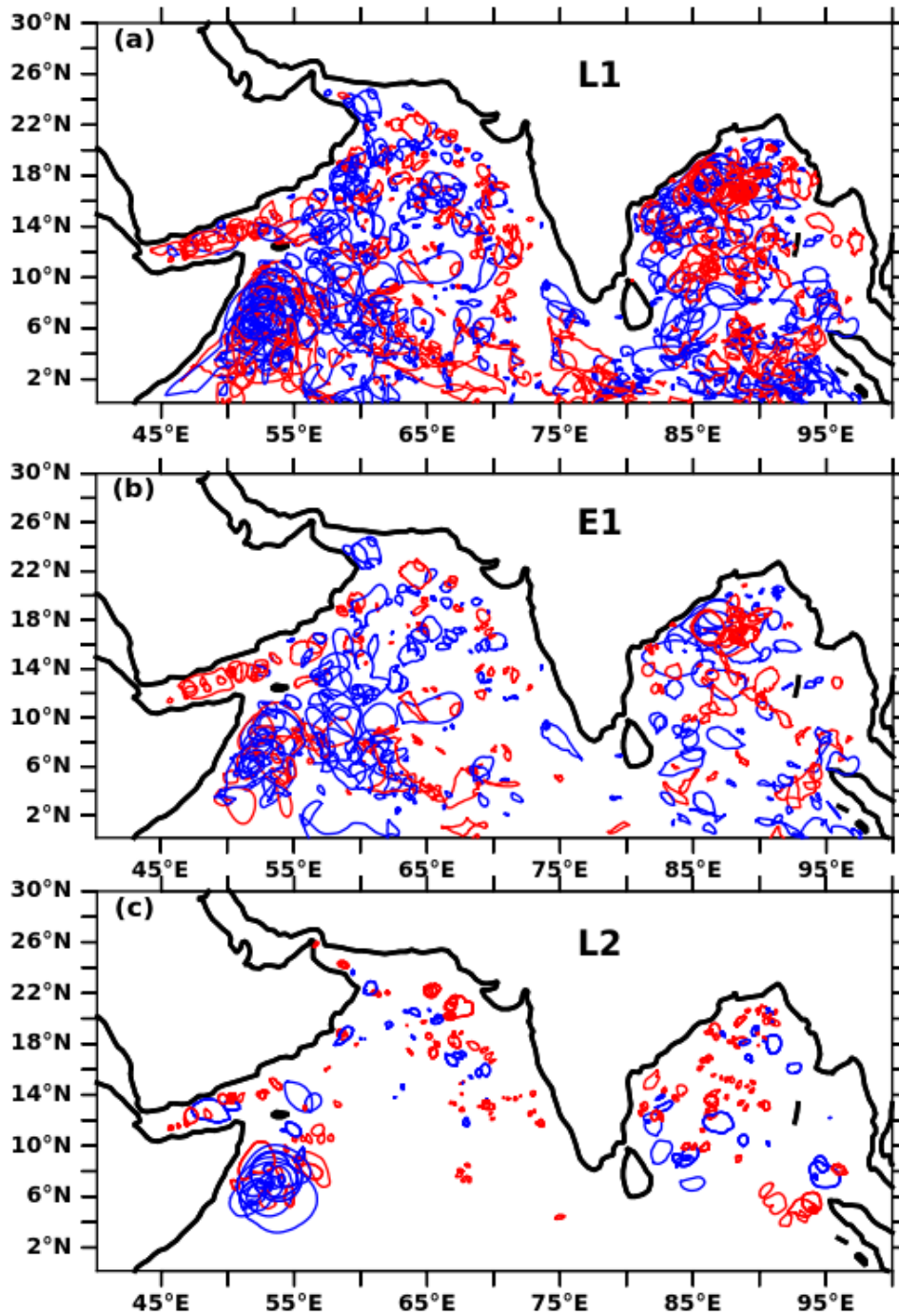


Figure 3. Trajectories of (a) L1 loops, (b) E1 eddies, and (c) L2 loops identified from loopers data provided by Lumpkin (2016). Blue and red color represents anticyclonic and cyclonic loops/eddies respectively.

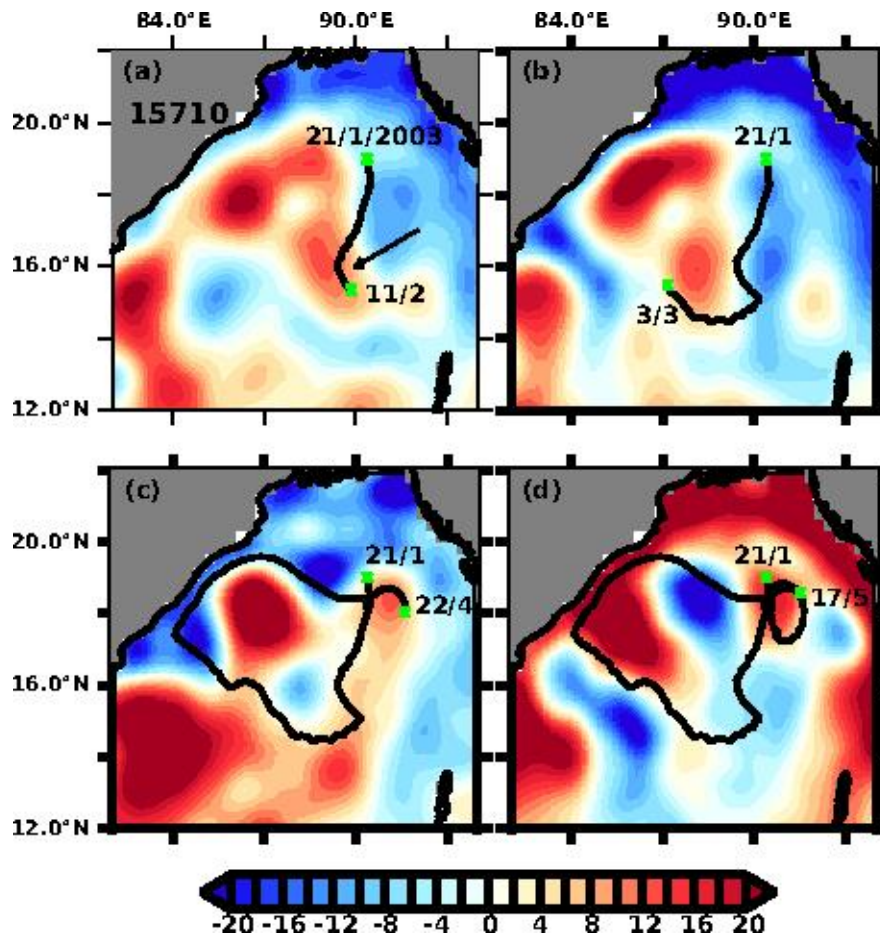


Figure 4. Trajectory of drifter with DAC No. 15710 and WMO id 2300593. Green cross provides the date of the position of the drifter in the trajectory, corresponding date and month of the position are also mentioned. An anticyclonic loop (L1) and an eddy (E1) are identified from this trajectory. Arrow in (a) points to location 16°N and 89°E, where the direction of rotation is changed. The colour panel shows the sea-level in cm on (a) 11 February 2003 (b) 3 March 2003 (c) 22 April 2003 (d) 17 May 2003.

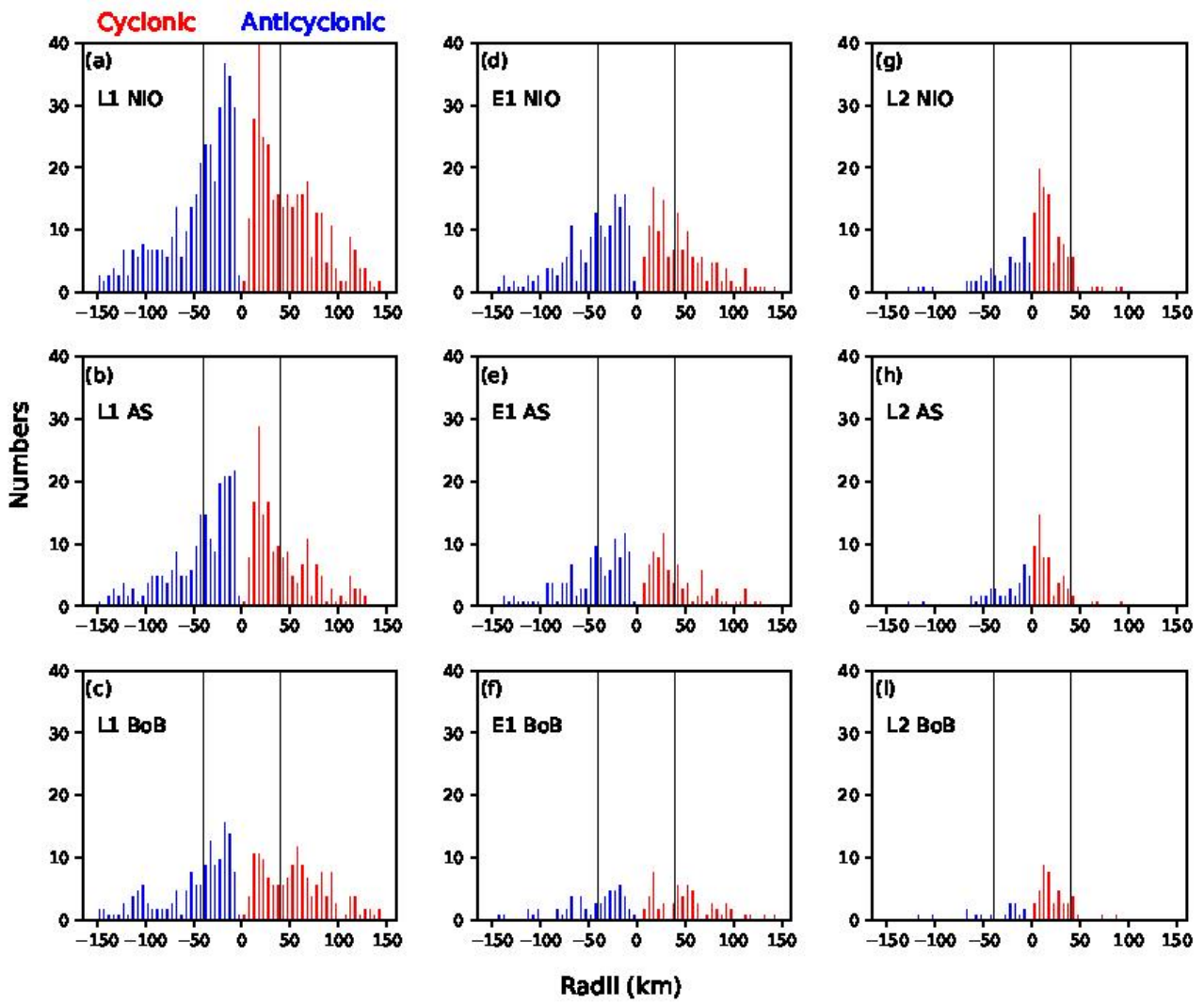


Figure 5. Histogram of radii for L1 loops for (a) NIO, (b) AS, and (c) BoB; E1 eddies for (d) NIO, (e) AS, and (f) BoB; L2 loops for (g) NIO, (h) AS, and (i) BoB. X axis denotes radii sizes in km and Y axis denotes number of loops/eddies. Blue and red color represents anticyclonic and cyclonic loops/eddies respectively. The black line at 40 km denote the approximate limit of satellite detection of eddies from sea-level.

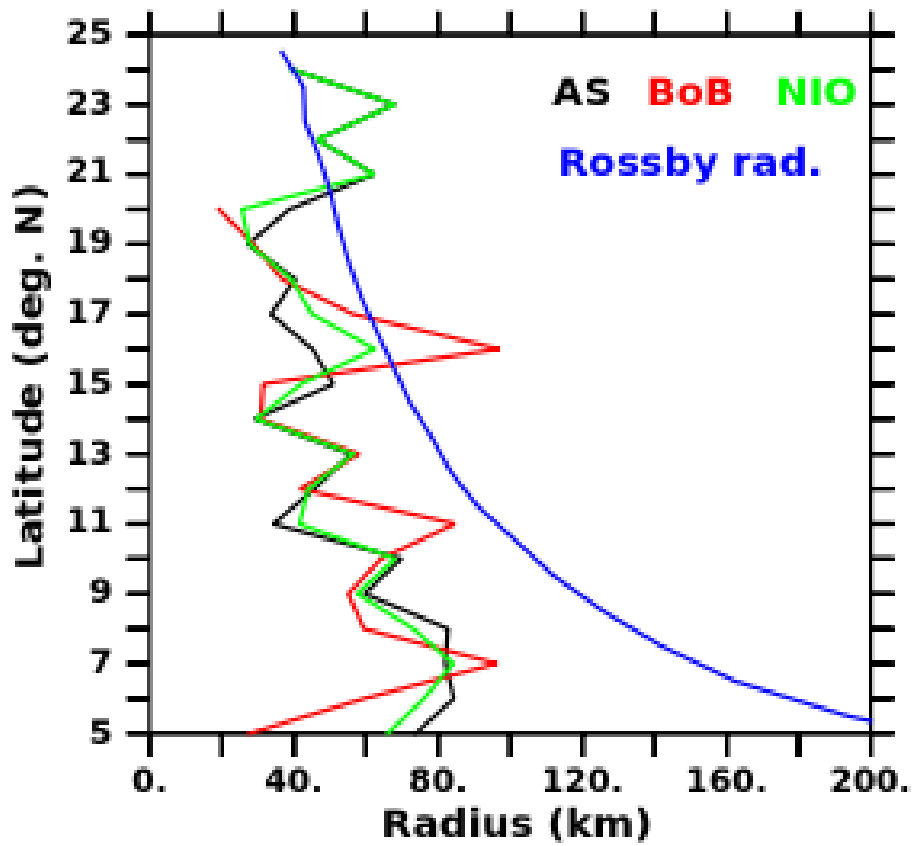


Figure 6. Average radius of eddy (E1) in AS, BoB and NIO in black, red and green respectively. Blue curve shows the values of Rossby radius of deformation (Chelton et al., 1998).

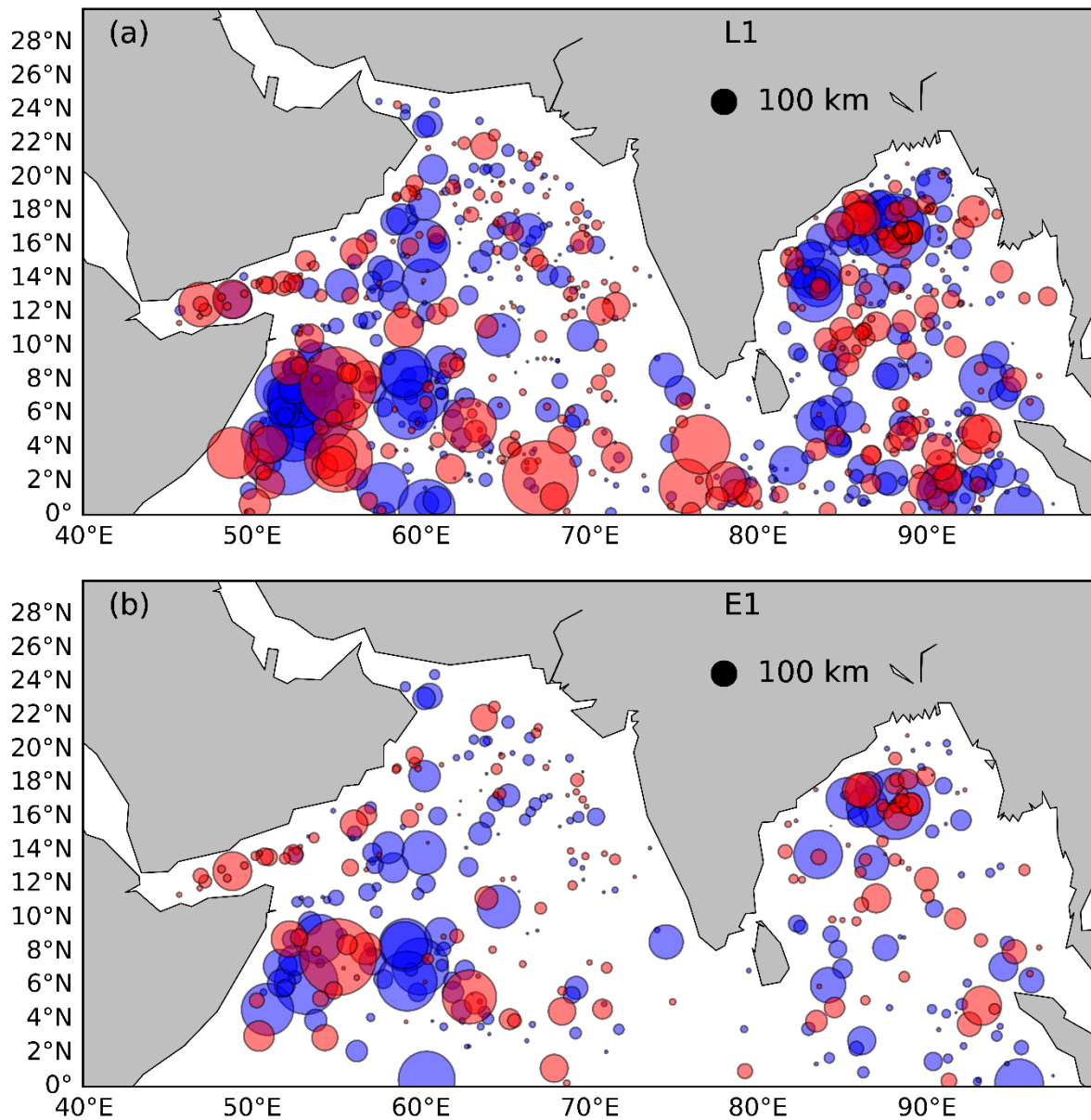


Figure 7. Spatial distribution of (a) L1 loops and (b) E1 eddies. Blue and red circles represents anticyclonic and cyclonic loops/eddies. The unit loop with 100 km radii is shown in black colour. All the other loops and eddies are plotted with reference to this unit loop.

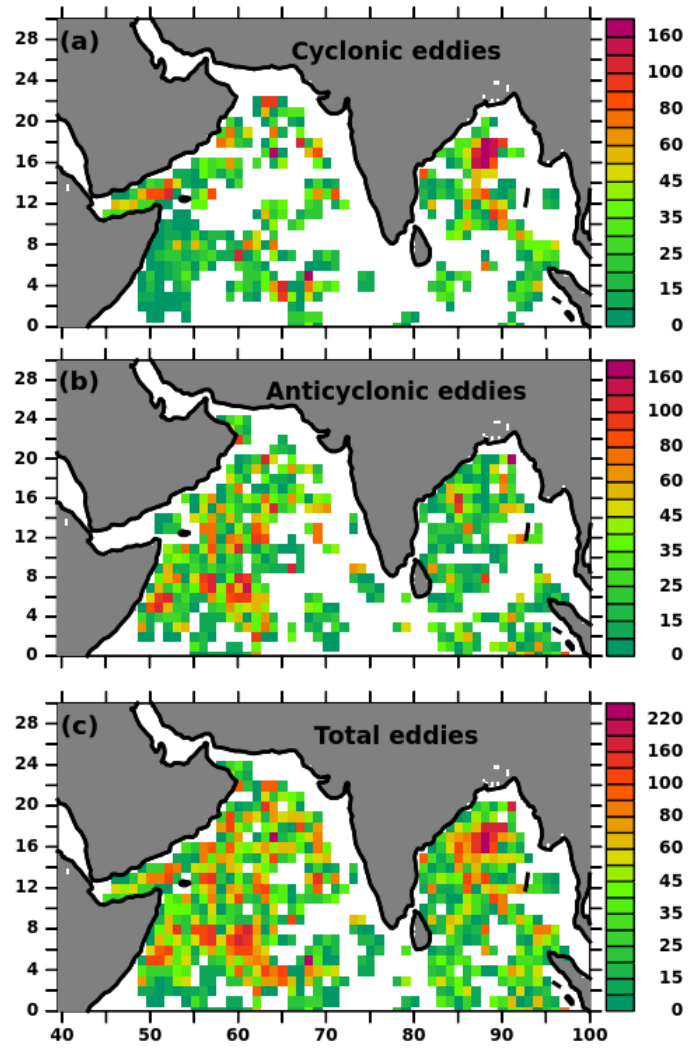


Figure 8. The number of eddy occurrences for (a) cyclonic, (b) anticyclonic, and (c) total (total of cyclonic and anticyclonic) eddies.

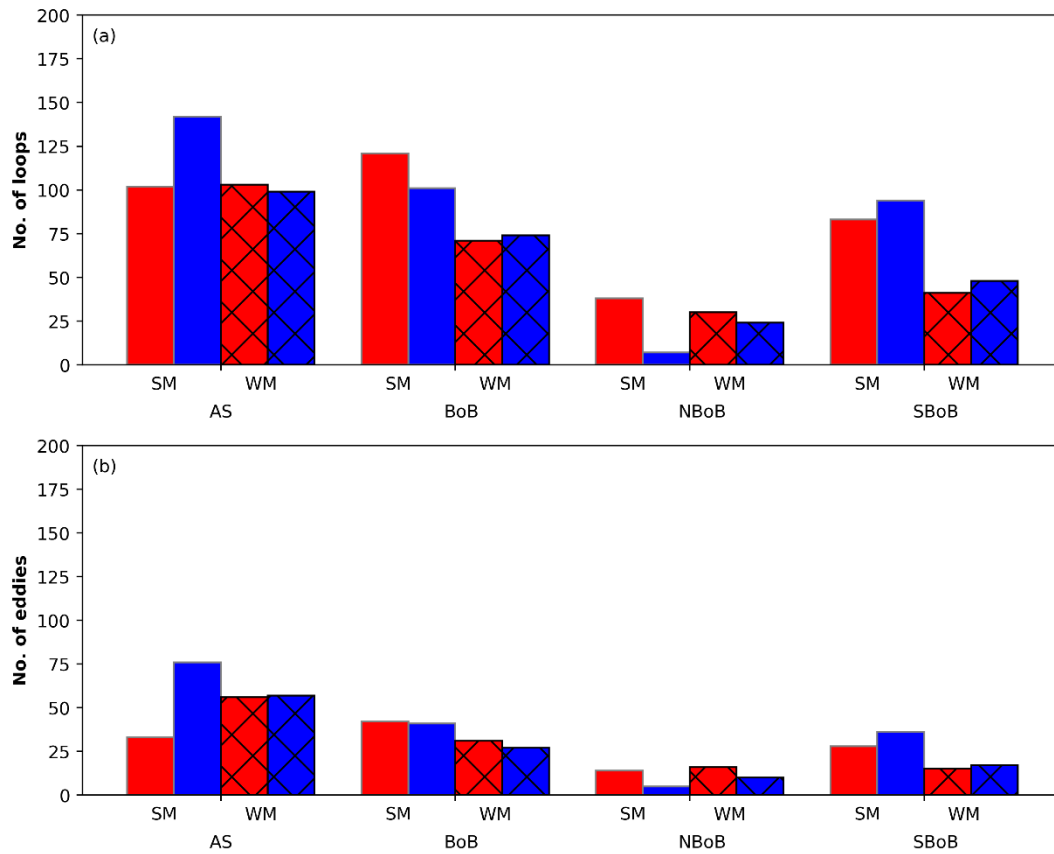


Figure 9. Number of cyclonic and anticyclonic (a) loops and (b) eddies, during Summer Monsoon (SM, June–September) and Winter Monsoon (WM, November–January) for AS, BoB, NBoB and SBoB. Blue and red bars represents anticyclonic and cyclonic loops/eddies.

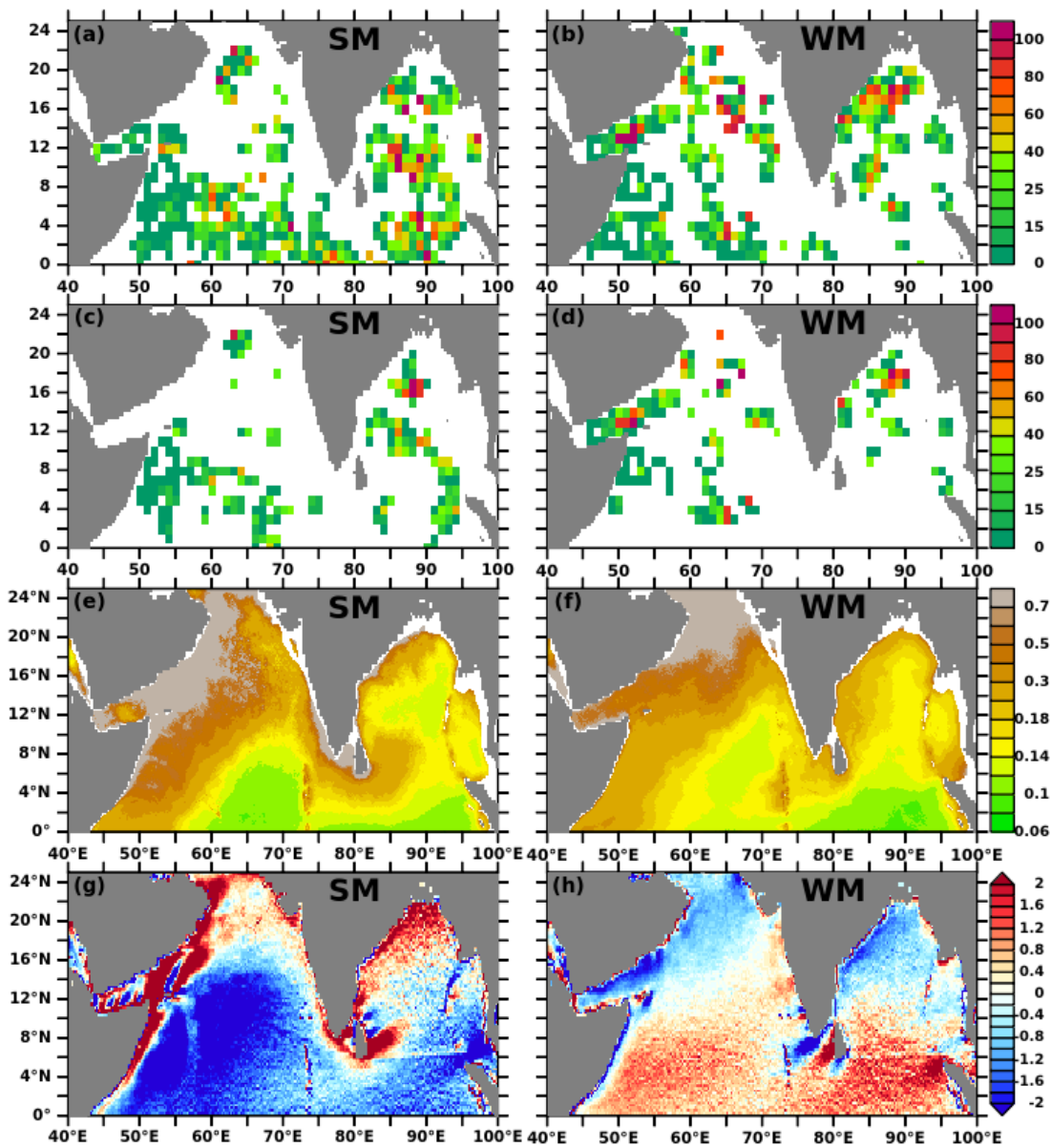


Figure 10. Number of cyclonic L1 loops during (a) Summer Monsoon (SM, June–September) and (b) Winter Monsoon (WM, November–January). Number of cyclonic E1 eddies during (c) SM and (d) WM. Chlorophyll during (e) SM and (f) WM. Wind-stress curl during (g) SM and (h) WM.

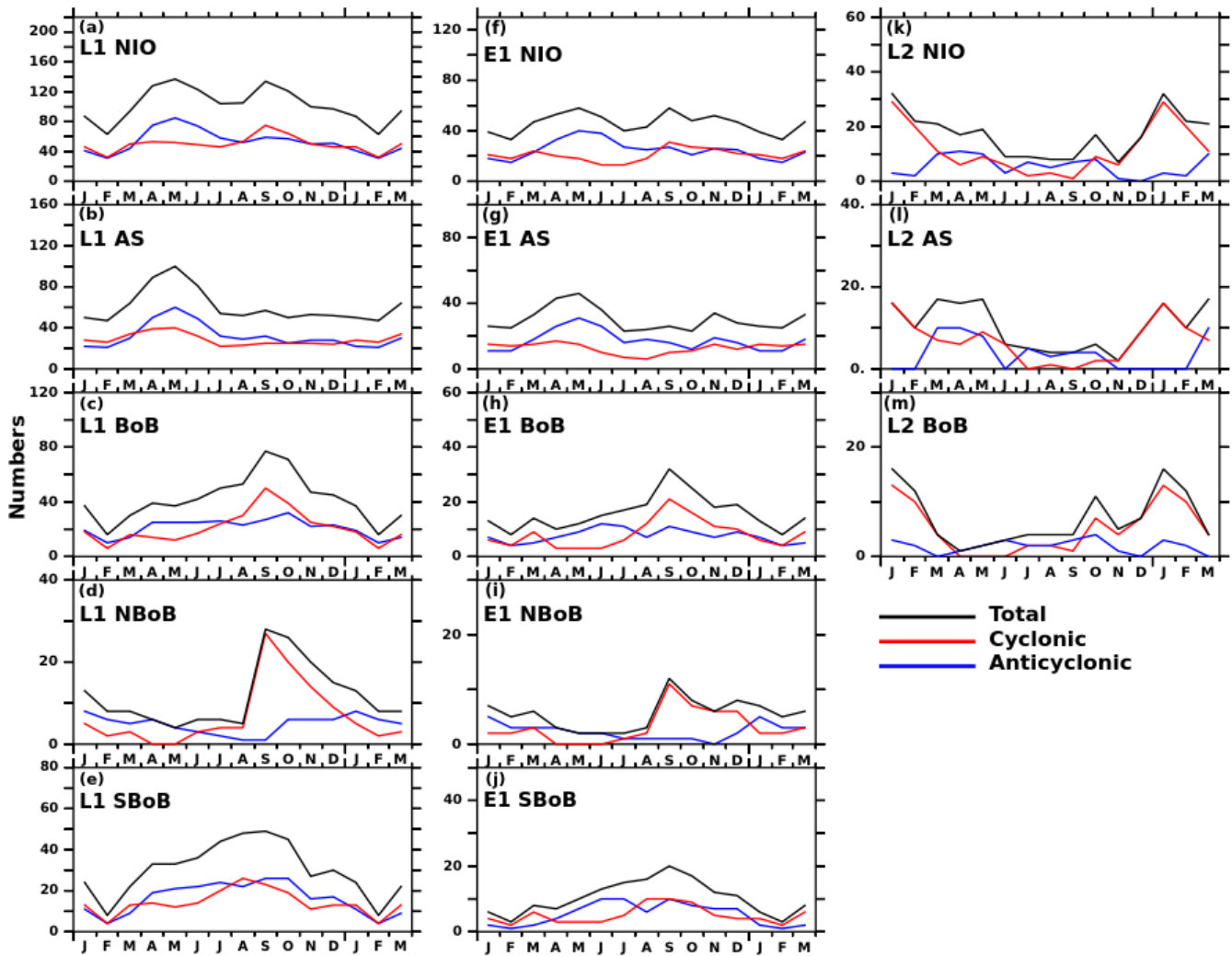


Figure 11. Temporal distribution of L1 loops for (a) NIO, (b) AS, (c) BoB, (d) NBoB and (e) SBoB; E1 eddies for (f) NIO, (g) AS, (h) BoB, (i) NBoB and (j) SBoB; L2 loops for (k) NIO, (l) AS, and (m) BoB. Here NBoB and SBoB refers to north and south of 16°N in BoB. Black, blue and red lines represents total (total of cyclonic and anticyclonic), anticyclonic and cyclonic loops/eddies respectively. The abscissa is taken from January to March for continuity.

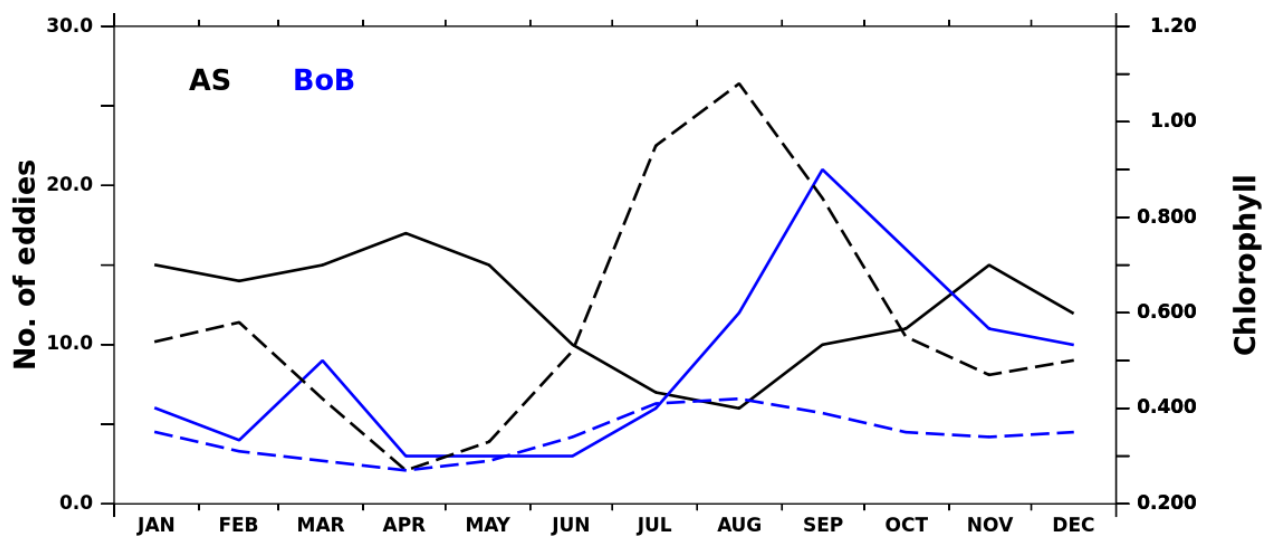


Figure 12. Temporal variability of cyclonic E1 eddies (solid lines) on the left Y-Axis. The right Y-axis shows the chlorophyll (dashed lines) in $mg\ m^{-3}$ for AS and BoB in black, and blue respectively.